Ab initio interionic potentials for CaO by multiple lattice inversion

Chao Wang[a,*], Shuo Zhang[a], Nan-Xian Chen[a,b]

[a] *Department of Physics, Tsinghua University, Beijing 100084, China*
[b] *Institute of Applied Physics, University of Science and Technology, Beijing 100083, China*

Abstract

Using Chen–Möbius inversion, we derive the interionic pair potentials from pseudopotential total-energy curves of the CaO crystals in B1, B3 and two P4/mmm virtual structures. Based on these potentials, the static properties of CaO in the rocksalt phase are calculated. Moreover, the phase stability of B1–CaO has been described by the energy minimizations from the disordered to the ordered states. Furthermore, the pressure-induced phase transition, phonon dispersion curves and properties of $(CaO)_n$ clusters have also been investigated. Compared with experimental data, most of our results indicate that the present calculated potentials are effective for studying properties of CaO ionic crystal.
© 2004 Elsevier B.V. All rights reserved.

Keywords: Calcium oxide; Ab initio calculation; Interionic potential; Lattice inversion

1. Introduction

Based on the Chen–Möbius inversion [1–4] and a series of pseudopotential total energy curves, the interionic pair potentials can be derived from multiple virtual structures [5]. Using the ab initio interionic potentials, the static properties of ACl (A = Li, Na, K, Rb), molecular dynamics simulations, temperature dependences of volume, bulk modulus and elastic constants are calculated. The results are in good agreement with the experimental values [6]. Not only the properties presented above but also the B1–B2 transition path in NaCl and RbCl, and the energies and stabilities of NaCl clusters are simulated. These are in excellent agreement with the experimental observations [7–9]. The successful results motivated us to use this concise and rigorous approach in simulating the properties of alkaline-earth oxides MgO, CaO, SrO, and BaO. These oxides have long been considered as a typical case for understanding bonding in ionic oxides and they are also one of the most fundamental materials for industrial application [10].

In the present work, we focus our interests on calcium oxide, CaO. CaO may be the most abundant component next

to the major components, MgO and SiO_2, in the Earth's lower mantle [11]. For this reason, considerable experiments have been paid to the elastic properties, static compression and equation of state, B1–B2 phase transition and high-temperature thermal expansion of CaO [12–16]. Several successful theoretical models have also been introduced to investigate the properties and behaviors of alkaline-earth oxides including CaO. For example, Potential-induced breathing model (PIB model) has calculated the second-order elastic moduli, high-pressure behavior, phonon dispersion, equations of state and B1–B2 phase-transition pressures of alkaline-earth oxides [17–19]. Breathing shell model (BSM) was used to examine the elastic constants, temperature dependences as well as the temperature–pressure–volume equation of states of both MgO and CaO [20]. Also, the elastic properties and pressure dependence of four B1-type alkaline-earth oxides were calculated using the ab initio full-potential linear muffin-tin-orbital (FP-LMTO) generalized gradient approximated (GGA) method to elucidate their systematics [10]. Transferable potential models of interatomic interactions in CaO, SrO, and BaO were obtained by fitting the forces and stress tensor given by the aspherical ion model (AIM) to predict thermal expansivities, elastic constants, phonon dispersion curves and pressure-driven phase transitions [21]. In most of the previous work [19–21], the interionic potentials

---

* Corresponding author. Tel.: +86-10-6277-2783;
fax: +86-10-6277-2783.

E-mail address: wangchao97@mails.tsinghua.edu.cn (C. Wang).

were started from the selection of interionic potential function forms with adjustable parameters, and then the potential parameters were obtained by fitting to the experimental data or calculation results. But our lattice-inverse potentials [5,6] are derived from ab initio calculations without any experimental data and priori potential function forms. This approach is more concise and convenient compared to other models and methods.

The paper is organized as follows: In Section 2, we introduce the scheme on how to derive the inversion interionic potentials from the total energies of CaO multiple lattices based on Chen–Möbius lattice inversion. Section 3 contains the application of our potentials to calculate the static properties, bulk modulus and elastic constants, stability of B1–CaO crystal. We also simulated the transition from the disordered to ordered CaO. As a further test of present potentials, phonon dispersion, B1–B2 phase-transition pressure and stability of CaO clusters are also presented in this section. All the results are discussed and compared with other models and experiments. Section 4 summarizes the results.

2. Description of inversion pair potential

2.1. Virtual structural models

In terms of the descriptions of pair potentials [22], the total energy $E_{tot}^{B1}(a)$ of B1 (NaCl-type) structure at lattice constant a can be expressed as Eq. (1), which includes three kinds of ionic interactions $E_{Ca-O}^{B1}(a)$, $E_{Ca-Ca}^{fcc}(a)$, and $E_{O-O}^{fcc}(a)$,

$$E_{tot}^{B1}(a) = E_{Ca-O}^{B1}(a) + E_{Ca-Ca}^{fcc}(a) + E_{O-O}^{fcc}(a) + E_{iso}, \quad (1)$$

where the $E_{Ca-Ca}^{fcc}(a)$ and $E_{O-O}^{fcc}(a)$ are the like-ion contributions on fcc (face-centered-cubic) sublattice, E_{iso} is the energy of isolated ions, which is independent of the interionic separation. As is known to us all, CaO initially exists in B1 (NaCl-type) structure that is expected to transform to B2 (CsCl-type) structure at high pressure [15]. Only with B1 and B2 structures, we cannot derive the inversion interionic potentials. So three other virtual structures (B3, T1, T2) are introduced with regard to B1 structure, which may not exist in nature, as shown in Fig. 1.
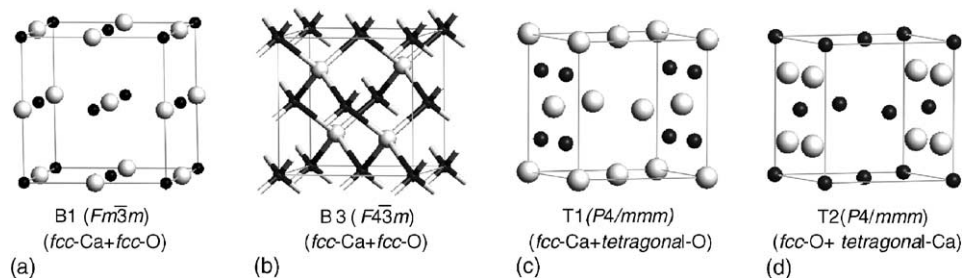
The total energy $E_{tot}^{B3}(a)$ of B3 (zinc blend structure) is

$$E_{tot}^{B3}(a) = E_{Ca-O}^{B3}(a) + E_{Ca-Ca}^{fcc}(a) + E_{O-O}^{fcc}(a) + E_{iso}. \quad (2)$$

If the four structures have the identical lattice constant a, from B1 to B3 only the cation-anion interaction undergoes the change for their identical like-sign ionic sublattices. The difference between B1 and B3 structures is only the relative displacement of cation and anion sublattices. From B1 to B3, the Ca–Ca and O–O distances are unaffected by this displacement, and their total-energy difference is only about the Ca–O interactions and can be expressed as

$$\Delta E_{Ca-O}(a) = E_{tot}^{B1}(a) - E_{tot}^{B3}(a) = E_{Ca-O}^{B1}(a) - E_{Ca-O}^{B3}(a). \quad (3)$$

Then the Ca–O pair potential curve can be evaluated by lattice inversion [3,4]. However, if the B2 (CsCl-type) model is selected, from B1 to B2, the Ca–O, Ca–Ca, and O–O interactions all undergo changes because cations and anions in the B2 structure are placed on the sc (simple cubic) sublattices. Therefore the combination of B1 and B2 structures could not give more information than the single B1 or B2 structure.

In order to obtain the O–O interaction from the total energies, the T1 structure is built as shown in Fig. 1(c), which consists of a cation fcc and an anion tetragonal sublattice. Its total energy can be expressed as

$$E_{tot}^{T1}(a) = E_{Ca-O}^{T1}(a) + E_{Ca-Ca}^{fcc}(a) + E_{O-O}^{tetra}(a) + E_{iso}. \quad (4)$$

For B1– and T1–CaO at the same lattice constant a, their cation–cation interaction $E_{Ca-Ca}^{fcc}(a)$ and $E_{Ca-Ca}^{fcc}(a)$ are identical, and their contributions from unlike-ion interactions can be separately calculated by the above Ca–O pair potential. Hence, the partial lattice energy as a function of the O–O pair potential can be derived from the total-energy difference between B1– and T1–CaO, which can be expressed as

$$\Delta E_{O-O}(a) = E_{tot}^{B1}(a) - E_{tot}^{T1}(a)$$
$$= E_{Ca-O}^{B1}(a) + E_{O-O}^{fcc}(a) - E_{Ca-O}^{T1}(a) - E_{O-O}^{tetra}(a). \quad (5)$$

Fig. 1. Structures used for ab initio pseudopotentials total-energy calculations. White balls denote cation (Ca^{2+}) positions and black balls show anion (O^{2-}) positions. (a) B1 (rocksalt) structure; (b) B3 (zinc blende) structure; (c) T1 structure (virtual structure for anion–anion interaction); (d) T2 structure (virtual structure for cation-cation interaction). Both B1 and B3 are formed by two fcc sublattices, and a fcc and a tetragonal sublattices are included in T1 and T2 structures.

As for the cation–cation interaction, the T2 structure as shown in Fig. 1(d) is generated by exchanging the atomic sites of cations and anions in the T1 structure. The T1 and T2 structures have the same space group P4/mmm. Then the total energy of T2–CaO is

$$E_{tot}^{T2}(a) = E_{Ca-O}^{T2}(a) + E_{Ca-Ca}^{tetra}(a) + E_{O-O}^{fcc}(a) + E_{iso}. \quad (6)$$

Similarly, the Ca–Ca partial lattice energy can also be obtained from the total-energy difference between B1– and T2–CaO.

As for the total energies of CaO crystals in B1, B3, T1, and T2 structures, they were calculated by using the LDA implemented in the CASTEP (Cambridge Serial Total Energy Package) program [23,24]. The norm-conserving pseudopotentials for Ca and O were used in this work. A plane-wave basis set with 560 eV cutoff was applied. The k-mesh points over the Brillouin zone were generated with parameters $4 \times 4 \times 4$ for the biggest reciprocal space and $1 \times 1 \times 1$ for the smallest one by the Monkhorst–Pack-scheme [25] corresponding to the lattice constant a. The energy tolerance for self-consistent field (SCF) convergence was 2×10^{-6} eV/atom for all calculations. Fig. 2 shows the calculated total energies of B1-, B3-, T1-, and T2-type CaO crystals as a function of crystal lattice constant a.

2.2. Ca–O interionic potential and three-body interaction model

According to Eq. (3), the total-energy difference between B1– and B3–CaO only depends on the Ca–O interaction, and can be rewritten as

$$\Delta E_{Ca-O}(a) = \Delta E_{Ca-O}^{Coul}(a) + \Delta E_{Ca-O}^{SR}(a), \quad (7)$$

in which $\Delta E_{Ca-O}^{SR}(a)$ is the short-range interaction, and $\Delta E_{Ca-O}^{Coul}(a)$ is the long-range Coulomb part between B1– and B3–CaO. According to the multiple lattice inversion [5], Coulomb interaction can be calculated by the fixed effective charges over a wide range of interionic distances but when we use the same approach on determining the effective charges of CaO, we find even if we regard the lattice energies approximately as only the sum of Coulomb potential when lattice constant $a \geq 10.0$ Å, the fixed ionic charges cannot be determined by fitting the total energy difference between B1– and B3–CaO at larger lattice constant. On the other hand, if we use the full ionic charges, 2.0e, as the effective charges, the non-Coulomb energy difference between B1– and B3–CaO at larger lattice constant is still different and the difference tends to a constant (Fig. 3). According to the result, we may conclude that this energy constant may be caused by many-body effect. So we introduced a three-body interaction model which is only relative to the angle between cation and anion [26]. The interaction can be expressed as

$$\phi_{ijk}(\theta) = C[1 - (-1)^n B \cos(n\theta_{ijk})], \quad (8)$$

where B and n are, respectively, 1 and 4. θ_{ijk} is the angle between ions i, j and k indicating the lattice sites of ions. C is the undetermined coefficient. For a determinate fabric, the three-body interaction can be determined only by the coefficient C and the interaction does not vary with lattice constant a because the three-body interaction is only relevant to the angle. For B1 structure, the three-body potential does not contribute to the total-energy on account of the 90° or 180° bond-angle while for B3 structure, the three-body angle energy is $4.736C$ per atom. For the model presented above, if the coefficient C has been determined, the short-range interaction can be ignored at larger lattice constant so the difference of three-body interaction energy between B1– and B3–CaO becomes
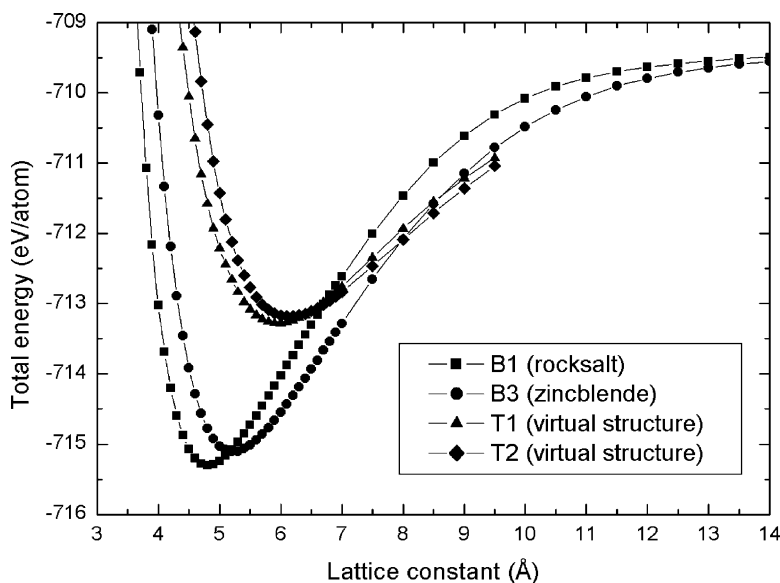

Fig. 2. Total energies in different CaO structures vs. lattice constant a from ab initio pseudopotentials calcultations.

a constant that can explain the invariant energy constant (see ΔE in Fig. 3) between B1 and B3 non-Coulomb interaction. According to this model, the non-Coulomb interaction can be regarded only as the sum of short-range two-body potential and three-body interaction,

$$E_{\text{non-Coul}} = \sum_{i,j} \phi(r_{ij}) + \sum_{i,j,k} \phi(\theta_{ijk}). \tag{9}$$

$$E^{\text{B1}}_{\text{Ca–O(SR)}}(a) = \frac{1}{2} \sum_{i,j,k} \phi^{\text{SR}}_{\text{Ca–O}} \left(\sqrt{(i+k-1)^2 + (i+j-1)^2 + (j+k-1)^2} \frac{a}{2} \right), \tag{12}$$

After introducing the three-body interaction model, we can rewrite Eq. (7) as

$$E^{\text{B3}}_{\text{Ca–O(SR)}}(a) = \frac{1}{2} \sum_{i,j,k} \phi^{\text{SR}}_{\text{Ca–O}} \left(\sqrt{\left(i+k-\frac{1}{2}\right)^2 + \left(i+j-\frac{1}{2}\right)^2 + \left(j+k-\frac{1}{2}\right)^2} \frac{a}{2} \right). \tag{13}$$

$$\Delta E_{\text{Ca–O}}(a) = E^{\text{B1}}_{\text{tot}}(a) - E^{\text{B3}}_{\text{tot}}(a)$$
$$= \Delta E^{\text{Coul}}_{\text{Ca–O}}(a) + E^{\text{SR}}_{\text{Ca–O}}(a) - E^{\text{B3}}_{\text{ang}}, \tag{10}$$

where $E^{\text{B3}}_{\text{ang}}$, a constant, is the three-body interaction energy of B3 CaO and $\Delta E^{\text{Coul}}_{\text{Ca–O}}(a)$, the difference of Coulomb energy between B1– and B3–CaO, can be calculated via the Madelung constants [27] of B1 and B3 structures or Ewald summation techniques [28] with the fixed ionic charges. The fixed ionic charges and C in three-body interaction model can be obtained by using Coulomb potential plus an undetermined constant to fit the total energy difference between B1– and B3–CaO at larger lattice constant. After the determination of the fixed charges q_+, q_- and constant C, the short-
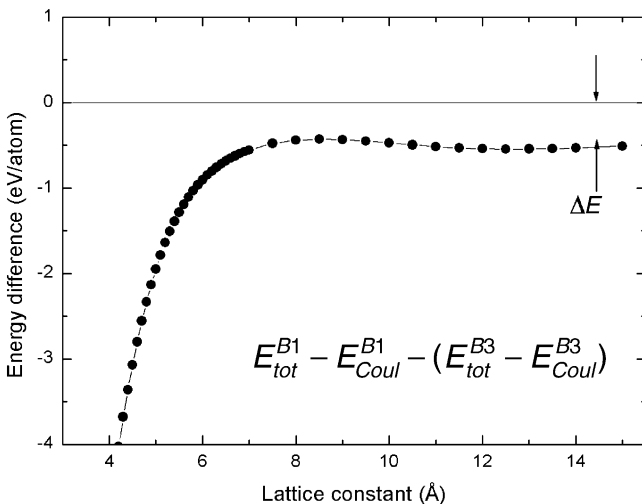

Fig. 3. The invariant energy constant ΔE between B1 and B3 non-Coulomb interaction at larger lattice constant.

range interaction difference between B1– and B3–CaO is

$$\Delta E^{\text{SR}}_{\text{Ca–O}}(a) = E^{\text{B1}}_{\text{Ca–O(SR)}}(a) - E^{\text{B3}}_{\text{Ca–O(SR)}}(a)$$
$$= E^{\text{B1}}_{\text{tot}}(a) - E^{\text{B1}}_{\text{Coul}}(a) - E^{\text{B3}}_{\text{tot}}(a)$$
$$+ E^{\text{B3}}_{\text{Coul}}(a) + E^{\text{B3}}_{\text{ang}}. \tag{11}$$

For the B1-type CaO, the short-range Ca–O interaction per ion can be expressed as

where the $\phi^{\text{SR}}_{\text{Ca–O}}$ is the Ca–O short-range pair potential, and the i, j, k indicate the atomic sites of ions in the unit of the lattice constant a. In the B3–CaO, the Ca–O short-range interaction per ion is

Thus, based on the Chen–Möbius lattice inversion [1–4], the interaction $\Delta E^{\text{SR}}_{\text{Ca–O}}(x)$ per ion can be expressed as the form as follows:

$$\Delta E^{\text{SR}}_{\text{Ca–O}}(x) = \frac{1}{2} \sum_{n} r_0(n) \phi^{\text{SR}}_{\text{Ca–O}}[b_0(n)x], \tag{14}$$

where x is the nearest-neighbor distance, $b_0(n)x$ is the nth-neighbor distance, and $r_0(n)$ is the nth coordination number. The series $\{b_0(n)\}$ is extended into a multiplicative semigroup. Then for any two integers m and n, there always exists an integer k such that

$$b(k) = b(m)b(n) \tag{15}$$

The $\Delta E^{\text{SR}}_{\text{Ca–O}}(x)$ can be rewritten as

$$\Delta E^{\text{SR}}_{\text{Ca–O}}(x) = \frac{1}{2} \sum_{n} r(n) \phi^{\text{SR}}_{\text{Ca–O}}[b(n)x] \tag{16}$$

where

$$r(n) = \begin{cases} r_0(b_0^{-1}[b(n)]) & \text{if } b(n) \in \{b_0(n)\} \\ 0 & \text{if } b(n) \notin \{b_0(n)\} \end{cases} \tag{17}$$

Thus the pair potentials $\phi^{\text{SR}}_{\text{Ca–O}}$ between Ca and O ions can be expressed as

$$\phi^{\text{SR}}_{\text{Ca–O}}(x) = 2 \sum_{n=1}^{\infty} I(n) \Delta E^{\text{SR}}_{\text{Ca–O}}[b(n)x], \tag{18}$$

in which the inversion coefficient $I(n)$ is given by

$$\sum_{b(n)/b(k)} I(n) r \left[b^{-1} \left(\frac{b(k)}{b(n)} \right) \right] = \delta_{k1}, \tag{19}$$

then the short-range Ca–O pair potential curve is obtained from lattice inversion as shown in Fig. 4. The shape of pair
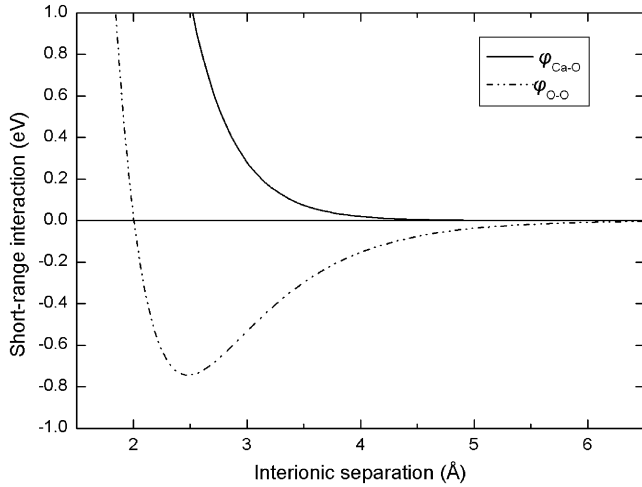
Fig. 4. Short-range interionic potentials for CaO.

potential curve indicates the repulsive exponential function form is suitable to express the Ca–O short-range interaction, and then the total Ca–O pair potential is

$$\Phi_{Ca-O}(r) = \phi_{Ca-O}^{SR}(r) + \phi_{Ca-O}^{Coul}(r)$$

$$= D_{+-} \exp\left[\gamma_{+-}\left(1 - \frac{r}{R_{+-}}\right)\right] + \frac{q_+ q_-}{4\pi\varepsilon_0 r}. \tag{20}$$

2.3. O–O interionic potential

Using the above inverted Ca–O pair potential, we can calculate the Ca–O interaction in B1– and T1–CaO crystals, respectively. Then the short-range O–O interaction difference between B1– and T1–CaO is obtained by

$$\Delta E_{O-O}^{SR}(a) = E_{O-O(SR)}^{B1}(a) - E_{O-O(SR)}^{T1}(a)$$

$$= E_{tot}^{B1}(a) - E_{Coul}^{B1}(a) - E_{Ca-O(SR)}^{B1}(a) - E_{tot}^{T1}(a)$$

$$+ E_{Coul}^{T1}(a) + E_{Ca-O(SR)}^{T1}(a). \tag{21}$$

The O–O short-range interaction per ion in B1–CaO can be expressed as

$$E_{O-O(SR)}^{B1}(a) = \frac{1}{4}\sum_{i,j,k\neq 0}\phi_{O-O}^{SR}$$

$$\times \left(\sqrt{(i+j)^2 + (i+k)^2 + (j+k)^2}\,\frac{a}{2}\right) \tag{22}$$

In the T1 structure, the Ca–O and O–O short-range interactions are separately defined as follows:

$$E_{Ca-O(SR)}^{T1}(a)$$

$$= \frac{1}{2}\sum_{i,j,k}\phi_{Ca-O}^{SR}$$

$$\times \left(\sqrt{\left(i+k-\frac{1}{2}\right)^2 + \left(i+j-\frac{1}{2}\right)^2 + (j+k)^2}\,\frac{a}{2}\right), \tag{23}$$

$$E_{O-O(SR)}^{T1}(a) = \frac{1}{4}\sum_{i,j,k\neq 0}\phi_{O-O}^{SR}\left(\sqrt{i^2 + 4j^2 + k^2}\,\frac{a}{2}\right). \tag{24}$$

By Chen–Möbius lattice inversion, the O–O short-range potential is calculated as Fig. 4. In terms of the curve shape, a Morse-stretch function form is selected for O–O short-range potential, and finally the O–O pair potential is

$$\Phi_{O-O}(r) = D_{--}\left(\left\{1 - \exp\left[\gamma_{--}\left(1 - \frac{r}{R_{--}}\right)\right]\right\}^2 - 1\right)$$

$$+ \frac{q_- q_-}{4\pi\varepsilon_0 r}. \tag{25}$$

2.4. Ca–Ca pair potential

By the similar method for O–O pair potential, the Ca–Ca pair potential can also be obtained. Based on our calculations, the short-range interaction between Ca ions is very small and can be neglected, thus the Ca–Ca interaction can be expressed only by Coulomb potential,

$$\Phi_{Ca-Ca}(r) = \frac{q_+ q_+}{4\pi\varepsilon_0 r}. \tag{26}$$

Finally, all the potential parameters have been obtained as given in Table 1.

3. Test for the interionic pair potentials

3.1. Static properties of CaO crystal

Using the above interionic potential from multiple lattice inversion, we first calculated the static properties of equilibrium B1–CaO at zero temperature and pressure. Static results for the lattice constant, lattice energy, bulk modulus, and elastic constants are shown in Table 2 together with a comparison to results obtained by aspherical ion model [21], potential-induced breathing model [17] and shell model (BSM) [20]. By comparison, the static results have also been calculated by COMPASS Forcefield [29] and other ab initio data [10], the experimental results are also listed in Table 2.

From Table 2, the calculated lattice constant, lattice energy of B1–CaO are in agreement with experimental results especially the lattice constant by present lattice inversion

Table 1
Interionic parameters derived by lattice inversion in this work

Non-Coulomb					Coulomb	
2-Body short-range interaction					3-Body	
Ion pair	Function form	D_{ij}(eV)	R_{ij}(Å)	γ_{ij}	C (eV)	Q_{eff}
−−	Morse	0.74426	2.47913	3.61839	0.030789	1.97539e
+−	Exp-repulsive	0.12485	3.30713	8.75162		

interionic potentials. In bulk modulus calculation, except the AIM [21] and PWPP-LDA [10] results, other potential models and ab initio calculations give small deviation from experimental results [12,17]. The result of bulk modulus by PIB model [17] is 10.5% lower than the experiment and BSM [20] gives 7.1%, FP-LMTO [10] gives 4.3% and LMTO-ASA LDA [10] gives 15.8% lower than the experiment respectively. The LAPW LDA [10] calculation gives the bulk modulus 13.2% larger than the experimental result, COMPASS [29] gives 22.8% and present potentials give 13.9% larger than the experimental result. The elastic constants depend on the second derivatives of the energy and thus a very accurate energy model is required to reproduce them accurately [21]. Although PWPP-LDA [10] reproduced good result on bulk modulus, it has not done well on C_{11} with 7.2% larger than experimental result and that is also subtly underestimated by PIB [17] with 7.6% and BSM [20] with 7.8% deviation respectively. The agreement of present result with experimental data is excellent with a deviation of 5.6% and the best calculated data is reproduced by COMPASS [29] (with a deviation of 0.4%) and AIM [21] (with a deviation of 3.9%). Both C_{12} and C_{44} results of present work and COMPASS are largely overestimated but present lattice inversion potentials reproduced the measured deviation from the Cauchy equality ($C_{11} = C_{44}$ for cubic crystals) successfully. The so-called Cauchy violation ($C_{11} \neq C_{44}$) cannot be reproduced by any

model based on two-body central forces, so our three-body interaction model can provide a good measurement of the many-body effect.

Besides the static properties of B1–CaO, another important test for the potential validity is using the potentials obtained from the properties of one phase to calculate the properties of other phases of a material. In this work we used the potentials from B1 and virtual structures to calculate the properties of B2 phase, while the B2 structure has not been used in the potential derivation. For comparison, the properties of B2–CaO have also been calculated based on the previous theories and experiment. All results are shown in Table 3.

The results of present work in Table 3 are seen to reproduce lattice constant more accurately at 60 GPa than the COMPASS Forcefield [29] compared with the experimental measurement [15]. The lattice constant, lattice energy and bulk modulus are also close to modified potential-induced-breathing (MPIB) model [19] and the First-principles calculation [30]. This shows that present interionic potentials have good transferability between B1 and B2 phases. The reason may be that our potentials were derived from the B1 and its related virtual structures, and this covers more configurations of phase space. Hence, despite that the B2 was not involved in the potential derivation, the potentials still well reproduced the properties of B2–CaO. From B2 to B2, this successful

Table 2
The equilibrium lattice constant, lattice energy (per molecule), bulk modulus and elastic constants of B1–CaO calculated by different interionic potentials and ab initio methods

	Lattice constant, a_0 (Å)	Lattice energy, E_{lattice} (eV)	Bulk modulus, B_0 (GPa)	Elastic constants (GPa)		
				C_{11}	C_{12}	C_{44}
Present work	4.842	34.92	129.8	235.5	77.0	99.2
COMPASS [29]	4.798	35.41	140.4	223.9	98.7	98.7
AIM [21]	4.809		116.1	231.9	58.2	73.0
PIB [17]	4.820	30.10	102.0	206.0	50.0	66.0
BSM [20][a]			105.9	205.6	56.1	79.4
FP-LMTO [10]	4.840		109.0	223.0	53.0	84.0
PWPP-LDA [10]	4.838		117.0	239.0	51.6	77.4
LAPW LDA [10]	4.714		129.0			
LMTO-ASA LDA [10]	4.650		96.0			
Experiment	4.810[b]	37.4[b]	114.0[c]	223.0[c]	59.0[c]	81.0[c]

Present work: lattice inversion interionic potentials of this work; COMPASS: COMPASS Forcefield of MSI [29]; AIM: aspherical ion model [21]; PIB: potential-induced breathing model [17]; BSM: breathing shell model [20]. The other theoretical [10] and experimental values [12,17] are also presented for comparison.
[a] Value at 500 K and 0 GPa.
[b] Room temperature data [17].
[c] Ultrasonic data [12].

Table 3
Static properties of B2–CaO calculated by lattice inversion interionic potentials, COMPASS Forcefield [29], and Modified potential-induced-breathing (MPIB) model [19] at 0 GPa and 60 GPa, respectively

	Lattice constant, a_0 (Å)	Lattice energy, $E_{lattice}$ (eV)	Bulk modulus, B_0 (GPa)
Present work[a]	2.955	32.9	154
COMPASS [29][a]	3.023	39.9	234
MPIB [19][a]	2.890	27.5	140
Tight-binding model [30][a]	2.973		
Present work[b]	2.727	32.1	154
COMPASS [29][b]	2.846	39.2	234
Experiment [15][b]	2.642		

Semiempirical tight-binding model [30] and experimental values [15] are also presented for comparison.

[a] At 0 GPa.
[b] At 60 GPa.

transferability implies the advantages of potentials from the extended phase space.

3.2. Stability of B1–CaO crystal

We took the structural stability as an important test for the present potentials. As a set of effective potentials, we think, the corresponding interionic forces should make the deformed structures recover to the equilibrium phase with the lowest energy. So based on the present interionic potentials, the energy minimization for deformed B1–CaO were performed by the conjugated gradient algorithm.

The detail of lattice deformation is described in Table 4. The deformed structures were constructed by randomly setting the lattice parameters, for example, the lattice constant a is from $0.3a_0$ to $1.8a_0$ (a_0 is the equilibrium lattice constant), the axial angle is even inclined to 27°, and some initial structures are constructed by simultaneously changing the lattice constants and axial angles. With the ten deformed B1–CaO's listed in Table 4, their energy minimizations were performed to search the stable configurations from these initial configurations.

After the energy minimizations, the final relaxed structures show that COMPASS and present potentials both exhibited good abilities for describing the stability of B1–CaO, as shown in Table 4. Only several deformed structures could not return to the equilibrium B1–CaO based on COMPASS potentials. This test suggests that present potentials appear promising in describing of the CaO crystal.

3.3. Transition from the disordered to ordered CaO

After testing the static properties of CaO crystal, we used this lattice inversion interionic potentials to describe the transition from the disordered to the ordered states in CaO. The disordered structure was built by randomly moving all ions 0.6 Å (25% of the nearest-neighbor distance) from their origin sites in a B1-type periodic supercell, which included 256 calcium ions and 256 oxide ions, as shown in Fig. 5 (a), then based on the conjugated gradient algorithm, the energy minimization led to the transition from disordered to ordered CaO, as shown from Fig. 5 (a)−(e). The corresponding radial distribution functions (RDFs) of intermediate configurations show the disordered gradually changes into the ordered states.

Table 4
Energy minimization results from the initial deformed to the final stable structures based on different interionic potentials in which the lattice parameters are in the units of their equilibrium values a_0, b_0, c_0, α_0, β_0 and γ_0

| Initial (unrelaxed)			Final (unrelaxed)	
a/a_0, b/b_0, c/c_0	α/α_0, β/β_0, γ/γ_0	Interionic potential	a/a_0, b/b_0, c/c_0	α/α_0, β/β_0, γ/γ_0
0.3, 1.0, 1.0	1.0, 1.0, 1.0	Present work	1.0, 1.0, 1.0	1.0, 1.0, 1.0
		COMPASS	1.0, 1.0, 1.0	1.0, 1.0, 1.0
1.8, 1.0, 1.0	1.0, 1.0, 1.0	Present work	1.0, 1.0, 1.0	1.0, 1.0, 1.0
		COMPASS	1.0, 1.0, 1.0	1.0, 1.0, 1.0
1.0, 1.0, 1.0	0.3, 1.0, 1.0	Present work	1.0, 1.0, 1.0	1.0, 1.0, 1.0
		COMPASS	Collapsed lattice	
0.3, 0.3, 0.3	0.6, 0.6, 0.6	Present work	1.0, 1.0, 1.0	1.0, 1.0, 1.0
		COMPASS	1.0, 1.0, 1.0	1.0, 1.0, 1.0
1.8, 1.8, 1.8	0.6, 0.6, 0.6	Present work	1.0, 1.0, 1.0	1.0, 1.0, 1.0
		COMPASS	Collapsed lattice	
0.3, 1.1, 2.0	0.9, 0.8, 1.1	Present work	1.0, 1.0, 1.0	1.0, 1.0, 1.0
		COMPASS	1.0, 1.0, 1.7	0.6, 0.6, 1.0
0.3, 0.3, 0.3	0.5, 0.6, 0.9	Present work	1.0, 1.0, 1.0	1.0, 1.0, 1.0
		COMPASS	1.0, 1.0, 1.0	1.0, 1.0, 1.0
0.5, 0.7, 0.9	0.6, 0.8, 1.2	Present work	1.0, 1.0, 1.0	1.0, 1.0, 1.0
		COMPASS	1.1, 1.1, 1.1	0.8, 0.8, 1.2
1.8, 1.8, 0.9	0.9, 0.7, 0.9	Present work	1.0, 1.0, 1.0	1.0, 1.0, 1.0
		COMPASS	2.2, 1.0, 1.0	1.0, 0.3, 1.0
1.5, 1.8, 0.8	0.8, 0.7, 1.1	Present work	1.0, 1.0, 1.0	1.0, 1.0, 1.0
		COMPASS	1.7, 1.0, 1.0	1.0, 0.6, 1.3
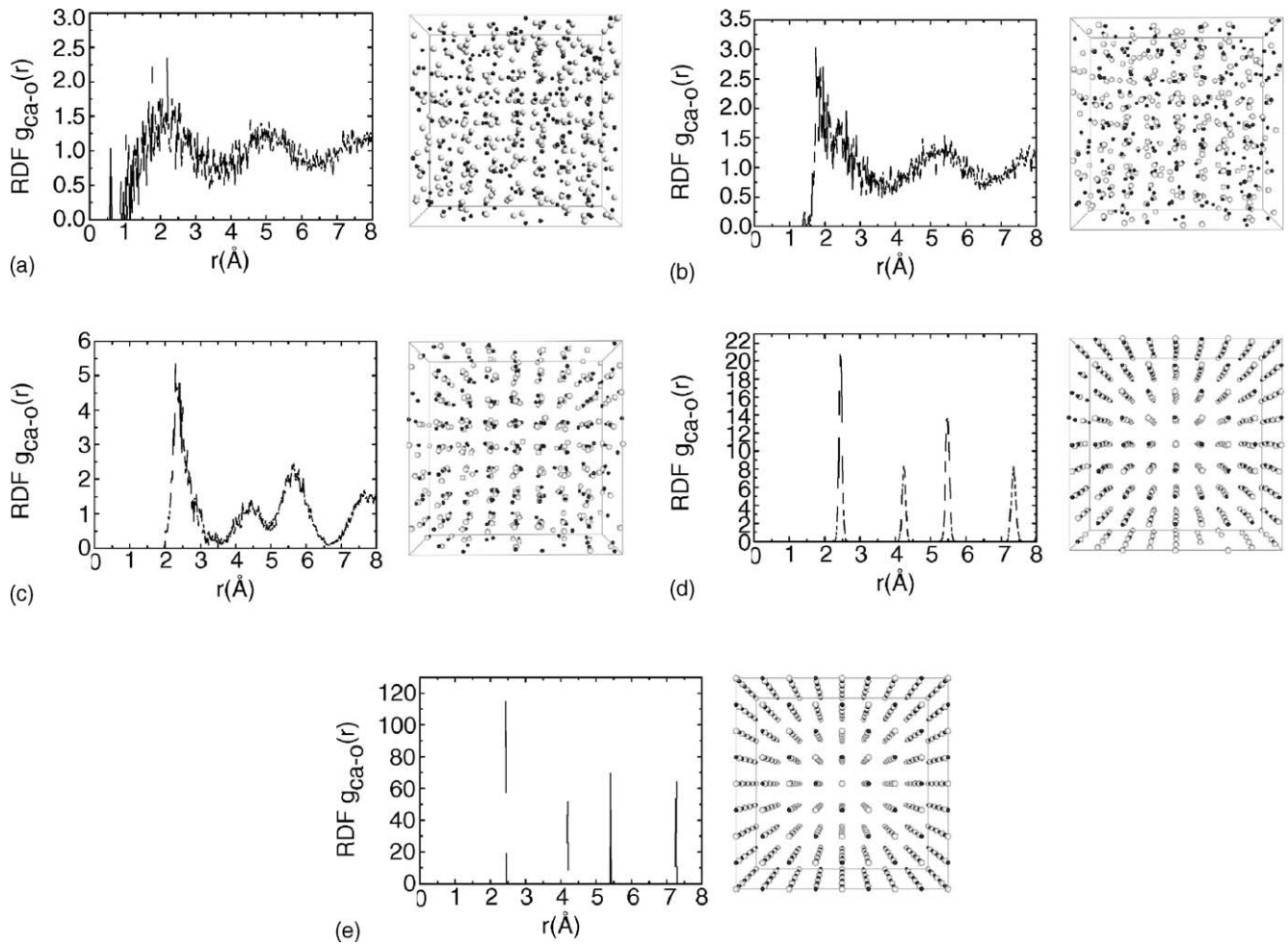
Fig. 5. Radial distribution function (RDF) and the corresponding configurations of the transition from disordered (a) to ordered CaO (e).

This transition may be considered as a special transition path from the molten CaO to the solid. As we know, it is very strict for the interionic potentials to make the disordered structure recover to the real equilibrium phase, especially the disor-dered phase is obtained by randomly moving all ions 0.6 Å from their equilibrium sites. Thus this transition indicates the present interionic potentials are valid over a wide range of interionic distance.
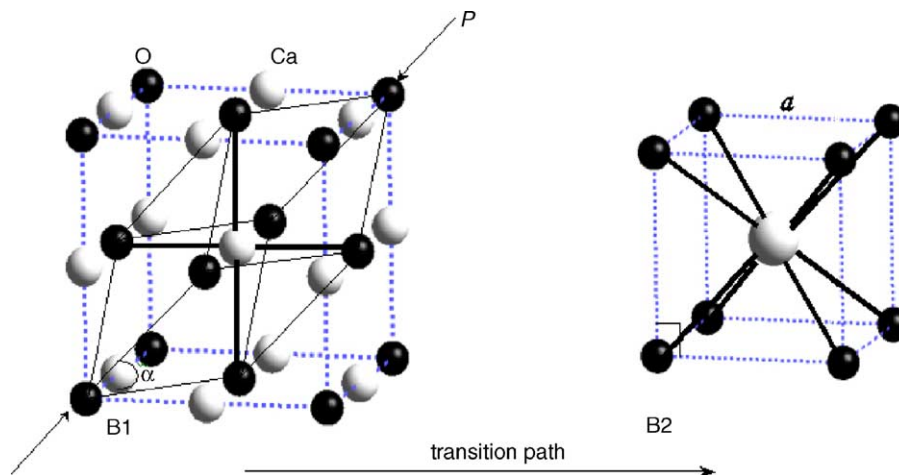

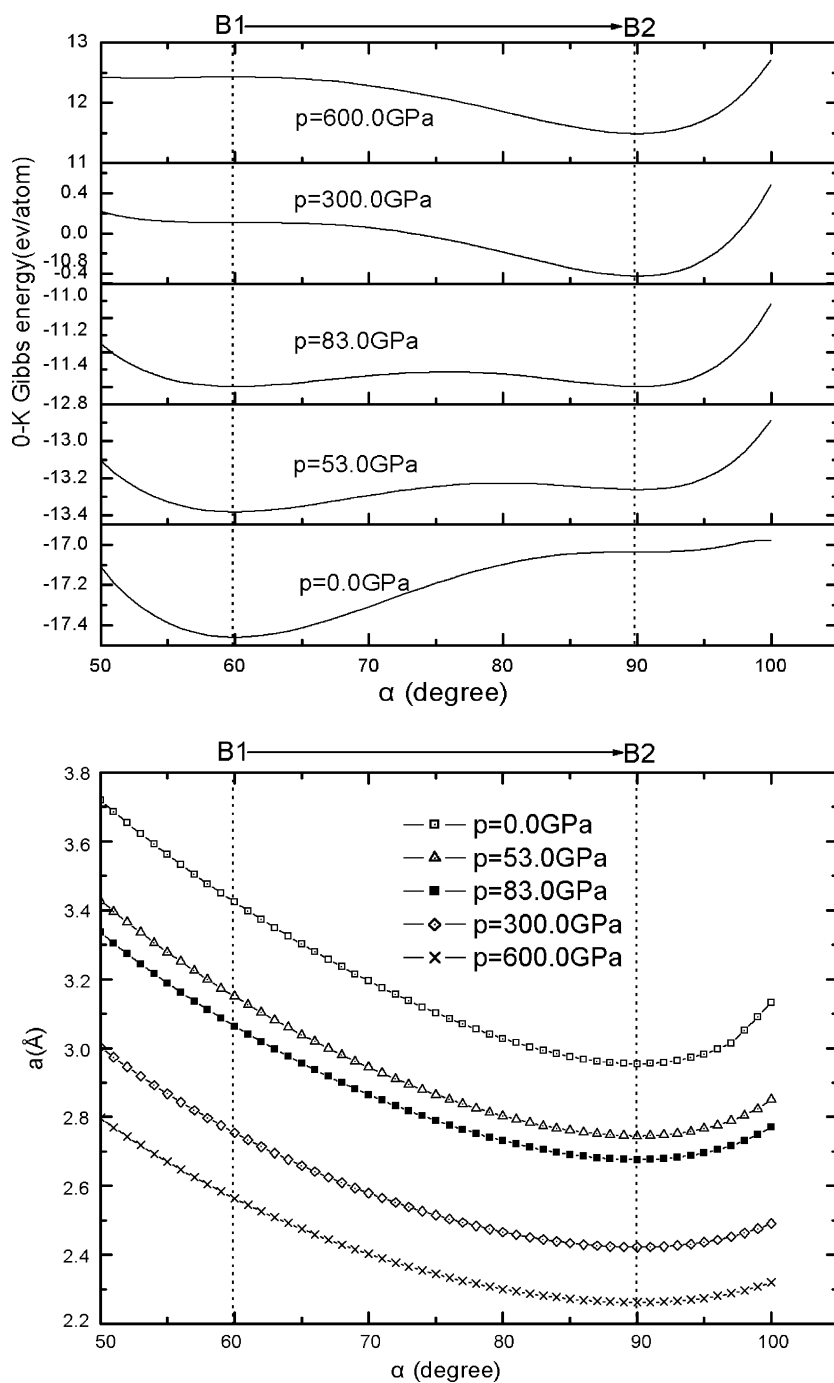Fig. 6. Transition path in two-ion cell for conversion of B1 into B2 phase.

Fig. 7. The 0 K Gibbs energy as a function of pressure *P* and rhombohedral angle *α* (a), and the corresponding *a*–*α* coupling along the transition path (b).

3.4. Pressure-induced phase transition

Calcium oxide, initially in the B1 (NaCl-type) structure, is expected to transform to the B2 (CsCl-type) structure at high pressure. There are considerable interests in such transitions both in theoretical and experimental studies of CaO [15,17,19,30–32]. Jeanloz et al. carried out shock-wave and diamond-cell techniques and demonstrated a B1–B2 transition in CaO at 60–70 GPa [15]. Majewski and Vogl predicted the structural phase transition pressure at about 70 GPa with

a tight-binding model by a total-energy-minimization procedure [30]. Sims et al. reported the transition pressure at about 70–94 GPa using both two-body potentials and first-principles periodic Hartree–Fock theory [31]. MPIB model calculated the phase-transition pressure of CaO at 61 GPa [19] which was calculated to be 55 GPa [17] with the PIB model and 83 GPa with an interionic potential by Singh and Sanyal [32].

In the present section, we attempt to predict the phase transition pressure of CaO by our lattice inversion interionic

potentials. The 0 K Gibbs free energies $G_0 = E + PV$ of B1 and B2 CaO can be calculated at different pressures. As is known to us all, the transition occurs at the pressure P_{tr} in which the Gibbs free energies of the two phases are equal. Therefore, based on the above inversion pair potentials, the Gibbs free energies of the intermediate structures were obtained. The details are described as follows.

If we assume the rhombohedral cell in Fig. 6 at a given external pressure P along the transition path, the 0 K Gibbs free energy surface versus cell angle α and cell length a could be calculated from the interionic pair potentials. That is to say, each of the intermediate structures was obtained by relaxing the initial cell $(a_0, a_0, a_0, \alpha, \alpha, \alpha)$ to the minimum-energy state $(a, a, a, \alpha, \alpha, \alpha)$ for each fixed angle α. This path in Fig. 7(a) shows that B1 and B2 are two local minima at zero pressure, and that B1 is lower than B2. With the increase of pressure P, the B1 and B2 states undergo the reverse changes, the first one rising from the minimum to the saddle point, and the second changing from a minimum to a deeper one. The coupling of the a, α coordinates along the transition path as a function of pressure P is shown in Fig. 7(b). At the transition pressure P_{tr} the Gibbs energy of B1 is the same as that of B2. Then the difference of Gibbs energy $\Delta G_0 = G_0(B1) - G_0(B2)$ per ion can be obtained by minimization of G_0 versus the cubic cell parameters for each phase at different pressures. From the equilibrium condition $\Delta G_0 = 0$ we can derive $P_{tr} = 83$ GPa as the transition pressure which is listed in Table 5, with theoretical and experimental data also listed for comparison [15,17,19,30–32].

These theories and experiment predict phase transition pressure varying from at least 55 GPa [17] to more than 90 GPa [19]. The results using the potential-based approach give larger data than the experiment [15]. The reason of present model may be that we overestimate the volume of

Table 5
Calculated and experimental phase transition pressures (GPa) between the B1 and B2 phase of CaO

Method	Transition pressure
Present model	83
PIB[a]	55
MPIB[b]	61
TB[c]	70
Buckingham[d]	93.7
HF[d]	70.4
Potential[e]	83
Experimental[f]	63

[a] Potential-induced breathing model [17].
[b] Modified potential-induced-breathing model [19].
[c] Tight-binding model [30].
[d] Buckingham potential and Hartree–Fock calculation [31].
[e] [32].
[f] [15].

B2 structure CaO at large pressure (see Table 3). So the phase transition pressure is larger than the experimental result.

3.5. Phonon dispersion curves for CaO

To fully test present potentials, we have obtained the phonon dispersion curve for CaO. This is an exacting test for potential models, as the phonons reflect the energetics of the crystal when the ions sample low-symmetry configurations [21]. We obtained the dispersion curve by gulp software [33] and the result is compared to experiment [34] in Fig. 8.

The lattice inversion interionic potentials gives excellent agreement with experiment for the acoustic modes but the LO branch is consistently too high as compared to experiment. As our potentials describe the stability of B1–CaO exceptionally well, this can explain the disagreement of LO branch. The
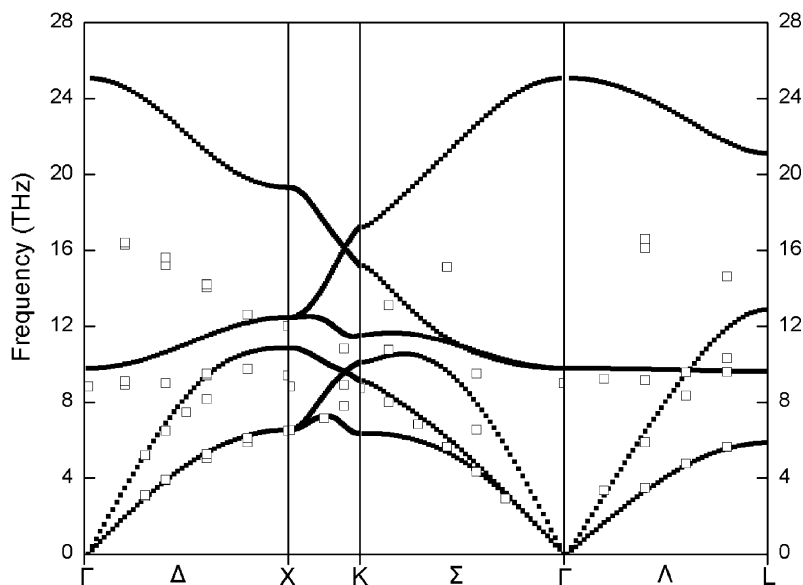

Fig. 8. Comparison of the calculated and experimental phonon dispersion for CaO. Circles represent experimental data [34].
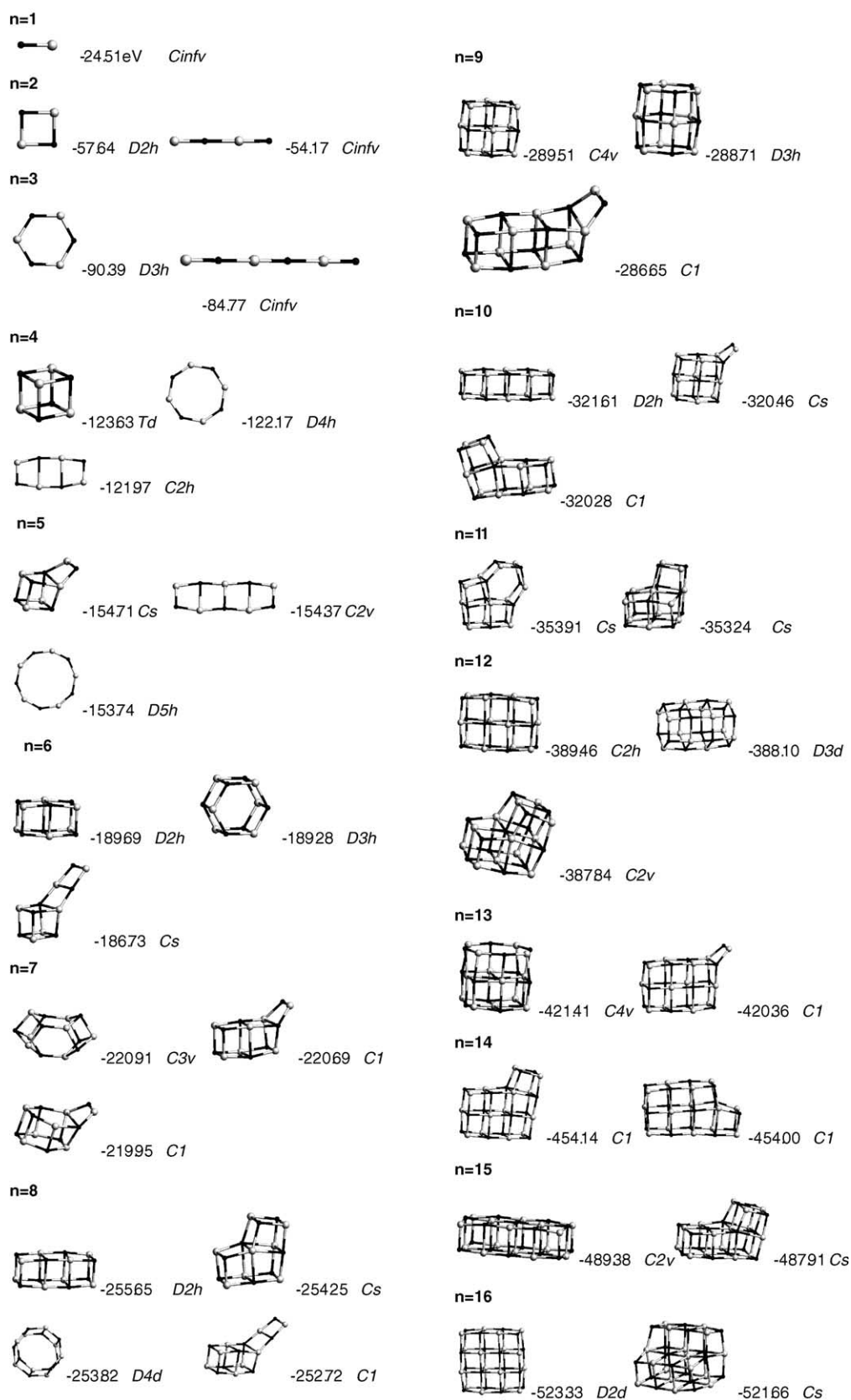
Fig. 9. The stable configurations, corresponding binding energies and point groups for (CaO)$_n$. The italics express the point groups. The binding energies are given in eV.

disagreement of optic branches also occurred obviously in the PIB model [18] and slightly in the AIM model [21] due to the neglect of dipolar charge relaxation.

3.6. Energies and stabilities of (CaO)$_n$ clusters

We have extended our study into energies and stabilities of neutral (CaO)$_n$ clusters using present lattice inversion interionic potentials. To our knowledge, none of the potential models and theoretical research which are discussed in the previous sections has given attention to this research. In previous work, a theoretical study of (CaO)$_n$ has been carried out by means of a semiempirical tight binding method and Malliavin and Coudray, etc. has compared its results with those obtained with ab initio calculations [35]. In the derivation of our interionic potentials, B1 (NaCl-type), B3 (CsCl-type), and two structures in space group P4/mmm named as T1 and T2 are simultaneously introduced in the pseudopotentials total energy calculations. This will lead to the interionic potentials including information from six-fold-coordinate B1 to four-fold-coordinate B3, T1 and T2. This may open a road to obtain the cluster-size independent pair potentials.

In our scheme, a fragment of B1–CaO is randomly chosen, and all ions in the fragment are randomly moved by 2.0 Å from their origin sites to form an initial cluster configuration. This routine is repeated 2000 times to produce an ensemble including 2000 initial configurations for the cluster (CaO)$_n$. Then the binding energy of CaO cluster is the sum of all over interionic pair potentials. According to energy minimization, each ion in clusters has to be adjusted to the minimum-energy position. The stable cluster configurations with different cluster sizes are consequently obtained corresponding to zero energy gradient at the minimum. Every cluster candidate configuration at different sizes is analyzed based on their binding energies and symmetries and the one with the lowest-energy is the most stable cluster. Consequently, the metastable clusters can also be found from the 2000 relaxed configurations according to their binding energies.

According to our scheme, the stable configurations of (CaO)$_n$ clusters (n = 1–16) are obtained as shown in Fig. 9. With these geometries, the binding energies are calculated over the all pair ionic interactions, and the corresponding point groups have also been determined within the tolerance of 0.01 Å. We made a comparison with DMOL calculations performed on neutral (CaO)$_n$ clusters by Malliavin and Coudray [35] and all the geometries of the clusters are in agreement with our calculations by lattice inversion interionic potentials from n = 1–6 except for n = 3. Our results indicate that the most stable cluster geometry of n = 3 is ring while Malliavin and Coudray's result is cubelike structure [35].

When n varies, the stabilities of the clusters with respect to their sizes are illustrated by the variations of the binding energies per molecule of the most stable structures. The binding energy per molecule have been shown in Fig. 10 from cluster size n = 2–16. As the function of cluster size n, the
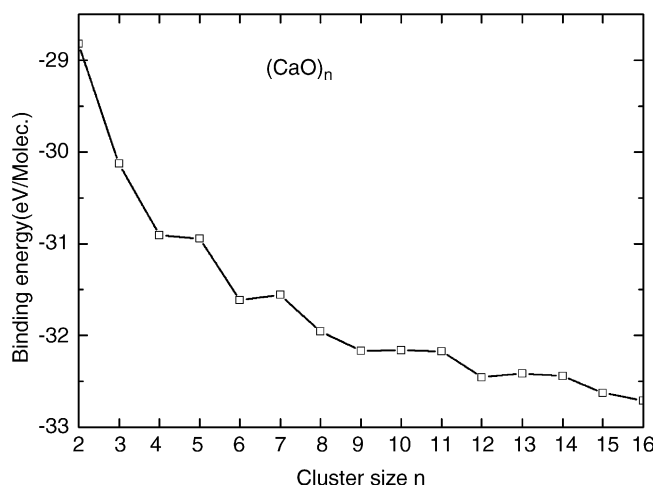

Fig. 10. Binding energy per molecule for the most stable configuration of (CaO)$_n$ clusters.

binding energy per molecule indicates that the clusters are relatively stable for n = 4, 6, 9, 12. These stable configurations also well agree with the ab initio calculation results [35]. This may demonstrate that the present pair potentials, with the simple potential function forms, can also provide the accurate results.

4. Conclusions

Based on the Chen–Möbius lattice inverse technique, the interionic pair potentials were derived from pseudopotentials total energy curves of bulk B1, B3, T1 and T2 virtual CaO crystals with their lattice constants covering from 4.0 to 14.0 Å. This scheme effectively extends the phase space of configurations beyond the equilibrium B1 structure, and then provides interionic interactions covering more configurations than that in conventional procedures. Through the combination of B1 and B3 structures, we derive ϕ_{Ca-O}^{SR} potential and the ionic charges Q_{eff} that is a fixed parameter for successive steps. Through the combination of B1 and T1 structures, we can derive ϕ_{O-O}^{SR} potential. Similarly ϕ_{Ca-Ca}^{SR} potential can be obtained by the combination of B1 and T2 structures. As the T1 and T2 are virtual structures, it is not difficult to build other virtual structures such as B10 (Fig. 11) to get the potentials. In this way, another set of potentials are obtained. That is to say different potential form can be produced from the choice of virtual structures. But no matter how different each potential is, the different sets of potentials give almost the same lattice constant, lattice energy, etc. The incomplete certainty of ionic charges Q_{eff} reflect the fact that the ions in crystal are not isolated any more since the charge distribution is obviously different from that of a free atom. In the present work, Q_{eff} is determined by fitting to the total-energy difference between B1– and B3–CaO crystals.

The main advantage of the present inverse method is that the extraction of these potentials are directly from ab initio
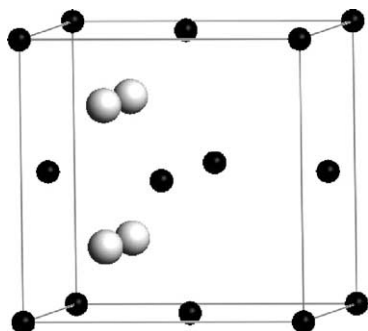
Fig. 11. B10 (*P4/nmm*) virtual structure.

calculations without any experimental data and priori potential function forms, so the potential functions could be selected in terms of the shapes of the inverted potential curves. This reduces some uncertainties in the derivation of pair potentials, such as prior assumption on potential functions Therefore our lattice inverse method is more concise and rigorous than other potential models. We derive fairly good results by such a wonderful method. The basic reason may be that the present pair potentials are originated from an extensive phase space, in which wide variations in coordination environment are concerned. It covers more ranges of coordination numbers, ionic bond lengths and angles. As present lattice inversion potentials are basically two-body potentials, such properties as the phase transition pressures, LO branch of the phonon dispersion curves have some disagreement with the experiment. But if a better three-body interaction potential is developed, we may have the confidence of better results. Therefore, these new interionic potentials may be promising in exploring and predicting the properties of ionic crystals and this new method is worth further refinement and extending to other ionic crystals.

Acknowledgment

References

[1] N.X. Chen, Phys. Rev. Lett. 64 (1990) 1193.
[2] J. Maddox, Nature 344 (1990) 377.
[3] N.X. Chen, Z.D. Chen, Y.C. Wei, Phys. Rev. E 55 (1) (1997) 5.
[4] N.X. Chen, X.J. Ge, W.Q. Zhang, F.W. Zhu, Phys. Rev. B 57 (1998) 14203.
[5] S. Zhang, N.X. Chen, Phys. Rev. B 66 (2002) 64106.
[6] S. Zhang, N.X. Chen, J. Chem. Phys. 118 (9) (2003) 3974.
[7] S. Zhang, N.X. Chen, Modell. Simul. Mater. Sci. Eng. 11 (3) (2003) 331.
[8] S. Zhang, N.X. Chen, Philos. Mag. 83 (2003) 1451.
[9] S. Zhang, N.X. Chen, Physica B 325 (2002) 172.
[10] T. Tsuchiya, K. Kawamura, J. Chem. Phys. 114 (2001) 10086.
[11] D.L. Anderson, Theory of the Earth, Blackwell Scientific Publications, Oxford, 1989.
[12] Z.P. Chang, E.K. Graham, J. Phys. Chem. Solids 38 (12) (1977) 1355.
[13] H. Oda, O.L. Anderson, D.G. Isaak, I. Suzuki, Phys. Chem. Miner. 19 (2) (1992) 96.
[14] P. Richet, H.-k. Mao, P.M. Bell, J. Geophys. Res. 93 (B12) (1988) 15279.
[15] R. Jeanloz, T.J. Ahrens, H.K. Mao, P.M. Bell, Science 206 (4420) (1979) 829.
[16] G. Fiquet, P. Richet, G. Montagnac, Phys. Chem. Miner. 27 (1999) 103.
[17] M.J. Mehl, R.J. Hemley, L.L. Boyer, Phys. Rev. B 33 (1986) 8685.
[18] R.E. Cohen, L.L. Boyer, M.J. Mehl, Phys. Rev. B 35 (1987) 5749.
[19] H. Zhang, M.S.T. Bukowinski, Phys. Rev. B 44 (1991) 2495.
[20] M. Matsui, J. Chem. Phys. 108 (1998) 3304.
[21] A. Aguado, L. Bernasconi, P.A. Madden, J. Chem. Phys. 118 (2003) 5704.
[22] V. Vitek, MRS Bull. 21 (2) (1996) 20.
[23] M.C. Payne, M.P. Teter, D.C. Allan, T.A. Arias, J.D. Joannopoulos, Rev. Mod. Phys. 64 (1992) 1045.
[24] V. Milman, B. Winkler, J.A. White, C.J. Pickard, M.C. Payne, E.V. Akhmatskaya, R.H. Nobes, Int. J. Quantum Chem. 77 (2000) 895.
[25] H.J. Monkhorst, J.D. Pack, Phys. Rev. B 13 (1976) 5188.
[26] S. Zhang, Ph.D. Thesis, Tsinghua University, Beijing, China, 2002.
[27] C. Kittel, Introduction to Solid State Physics, seventh ed., Wiley, New York, 1996.
[28] P.P. Ewald, Ann. Phys. (N. Y.) 64 (1921) 253.
[29] H. Sun, J. Phys. Chem. B 102 (1998) 7338.
[30] J.A. Majewski, P. Vogl, Phys. Rev. Lett. 57 (1986) 1366.
[31] C.E. Sims, G.D. Barrera, N.L. Allan, W.C. Mackrodt, Phys. Rev. B 57 (1998) 11164.
[32] R.K. Singh, S.P. Sanyal, Phys. Status Solidi B 113 (1982) 23.
[33] J. Gale, Department of Chemistry, Imperial College, South Kensington, London, SW72AY. email: j.gale@ic.ac.uk, http://www.ch.ic.ac.uk/gale/Research/gulp.html.
[34] D.H. Saunderson, G. Peckham, J. Phys. C 4 (14) (1971) 2009.
[35] M.J. Malliavin, C. Coudray, J. Chem. Phys. 106 (6) (1997) 2323.